Relating pore fabric geometry to acoustic and permeability anisotropy in Crab Orchard Sandstone: A laboratory study using magnetic ferrofluid

Philip M. Benson, Philip G. Meredith, and Ellen S. Platzman
Department of Earth Sciences, University College London, London, UK

Received 10 June 2003; revised 29 August 2003; accepted 4 September 2003; published 3 October 2003.

[1] Pore fabric anisotropy is a common feature of many sedimentary rocks. In this paper we report results from a comparative study on the anisotropy of a porous sandstone (Crab Orchard) using anisotropy of magnetic susceptibility (AMS), acoustic wave velocity and fluid permeability techniques. Initially, we characterise the anisotropic pore fabric geometry by impregnating the sandstone with magnetic ferro-fluid and measuring its AMS. The results are used to guide subsequent measurements of the anisotropy of acoustic wave velocity and fluid permeability. These three independent measures of anisotropy are then directly compared. Results show strong positive correlation between the principal directions given from the AMS, velocity anisotropy and permeability anisotropy. Permeability parallel to the macroscopic crossbedding observed in the sandstone is 240% higher than that normal to it. P and S-wave velocity anisotropy and AMS show mean values of 19.1%, 4.8% and 3.8% respectively, reflecting the disparate physical properties measured. *INDEX TERMS:* 5102 Physical Properties of Rocks: Acoustic properties; 1518 Geomagnetism and Paleomagnetism: Magnetic fabrics and anisotropy; 5139 Physical Properties of Rocks: Transport properties; 5114 Physical Properties of Rocks: Permeability and porosity. **Citation:** Benson, P. M., P. G. Meredith, and E. S. Platzman, Relating pore fabric geometry to acoustic and permeability anisotropy in Crab Orchard Sandstone: A laboratory study using magnetic ferrofluid, *Geophys. Res. Lett.*, *30*(19), 1976, doi:10.1029/2003GL017929, 2003.

1. Introduction

[2] Pore fabric geometry is one of the primary factors affecting fluid flow in porous media. Pore fabric anisotropy, which may result from depositional layering, diagenesis or subsequent microcracking have all been shown to play important roles in influencing the petrophysical properties of rock [*Lo et al.*, 1986; *Jones and Meredith*, 1998; *Rasolofosaon and Zinszner*, 2002]. Acoustic wave velocity measurement has proven to be a useful tool for estimating porosity and anisotropy [*Wyllie and Gregory*, 1958]. However, the relationship between the measured quantity, velocity, and the actual permeability remains non-trivial. Pore space geometry may be inferred from velocity measurements by assuming that acoustic velocity is directly related to the amount of void space crossed by the wave [*Berge et al.*, 1992]. However, the assumption that all void spaces affect velocity equally may not be valid, especially for cracked media. Classically, velocity anisotropy has been studied in 2-D, using cylindrical core samples [*Jones and Meredith*, 1998; *Louis et al.*, 2003]. More recently, 3-D approaches have become possible through the complex procedure of machining spherical samples [*Durrast et al.*, 2002].

[3] In this work, we use the method of anisotropy of magnetic susceptibility (AMS) to characterize and quantify the AMS of the solid matrix (mAMS) and the AMS of the ferrofluid saturated pore space (pAMS) [*Pfleiderer and Halls*, 1990; 1994] of an anisotropic sandstone. By taking samples along the major anisotropy axes identified by pAMS we then compare and contrast the pAMS method with both the acoustic and permeability methodologies. The results allow us to define the relationships between the size and shape of the void space geometry and the anisotropy of acoustic velocity and fluid permeability. We also show that pAMS is a more accurate method for estimating the principal directions of the anisotropy of acoustic wave velocity and permeability for our sample material. We discuss the results in terms of the sedimentary microstructure and their ability to elucidate petrophysical properties of the samples.

2. Experimental Method

[4] The sample material used was Crab Orchard Sandstone, from the Cumberland plateau, Tennessee, USA. It is a red, fine-grained, crossbedded fluvial sandstone. Grains are generally subhedral to subrounded, approximately 0.25 mm in size, showing no preferred alignment. Porosity is 5% ± 0.5%. Compositionally, the rock is predominantly quartz (over 85%), with feldspar, lithics and an abundant cement of sericitic clay. All samples used in this study were prepared from a single block of material, cored in one of three orthogonal directions (Figure 1). The three directions correspond to the faces of the block as received from the quarry; with 'X' and 'Y' approximately parallel to bedding and 'Z' approximately normal to it.

[5] AMS measurements were made on cylindrical samples 25.4mm in diameter and ~22mm in length, corresponding to a length/diameter ratio of ~0.88. This is the standard geometry used in palaeomagnetic studies as it minimises the shape dependent demagnetizing effect observed in samples with high intensity of magnetization [*Pfleiderer and Halls*, 1990; *Tarling and Hrouda*, 1993]. To evaluate pAMS, samples were saturated with ferro-fluid EMG-905 (Ferrotec Corporation), which is a colloidal suspension of superparamagnetic magnetite particles (10nm mean diameter) held in a light mineral oil carrier fluid. The particles are kept in suspension by

0094-8276/03/2003GL017929

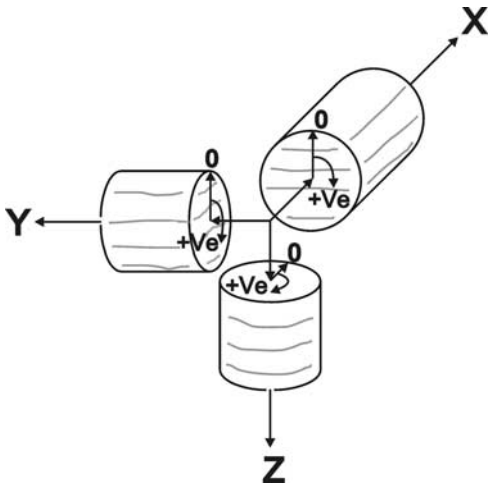

Figure 1. Co-ordinate system used in this study; Z is normal to bedding, and X and Y are parallel to bedding.

Brownian motion, and are coated with a stabilising dispersing agent that prevents agglomeration. The ferrofluid was diluted by a factor of 5 with additional carrier fluid, giving a final susceptibility of 0.35 SI. This keeps the bulk susceptibility of the saturated rock samples within measurable range and minimises demagnetization effects. Samples were saturated by vacuum immersion for 12 hours.

[6] The magnetic susceptibility was then measured in 15 directions using a KLY-2 susceptibility bridge (AGICO Instruments). The principal susceptibility axes were calculated by inverting the tensor for the 3-D ellipsoid using a least square method [*Jelinek*, 1978]. Although a minimum of only six measurements is needed to fully define the susceptibility tensor the use of 15 independent readings allows statistical evaluation of errors in the three principal directions.

[7] Acoustic wave velocity measurements were made on samples 38.1mm in diameter by ~40 mm long, cored along the same three orthogonal directions as for the AMS samples. Acoustic velocities were measured radially in 10° increments via the pulse transmission method [*Birch*, 1960; *Ayling et al.*, 1995], using 1MHz transducers. The combination of grain and sample size ensured a minimum of 10 grain diameters per wavelength and 10 wavelengths across the sample diameter. A 900 volt pulser was used to excite the transmitting transducer, received waveforms were recorded and displayed on a digital storage oscilloscope. We estimate the absolute accuracy of picked velocities as ~1% for P-waves and ~2% for S-waves. However, the accuracy of velocity variation is higher; estimated at 0.4%.

Table 1. Bulk Susceptibility (χ), $\times 10^{-6}$ SI (27 Samples)

	Dry matrix	Ferrofluid saturated sample
Average	46.2	13583
Std. deviation	27.8	2864

[8] Permeability was measured both parallel and perpendicular to bedding on a sub-set of the samples used for velocity measurement. Measurements were made in a servo-controlled steady-state-flow permeameter [*Jones and Meredith*, 1998]. Two servo-controlled fluid pressure intensifiers were used to maintain a small, constant pressure differential (0.5 MPa) across jacketed samples. Permeability is calculated directly from the fluid volume flow rate via Darcy's Law. The pore fluid used was distilled water and all measurements were made at an effective pressure of 5MPa.

3. Results

[9] Measurements of the initial, bulk magnetic susceptibility of dry Crab Orchard sandstone gives a low value accounting for only ~0.3% of the bulk susceptibility of the ferrofluid saturated rock (Table 1). pAMS measurements of the saturated samples are therefore overwhelmingly a reflection of the anisotropy of void space geometry, rather than grain fabric. In addition, the magnitude of total susceptibility reflects the total volume of ferro-fluid in the sample. Since the bulk volume of the sample is known, the ratio of the two volumes gives an independent measure of sample porosity. The calculated 'susceptibility porosity' was 4.4 ± 1.2%, comparing well with the gravimetric porosity of 4.9 ± 0.2%. Figure 2a shows a lower hemisphere stereographic projection of the principal pAMS directions obtained from measurements on 27 saturated samples, 9 cored along each of the X, Y, and Z directions. After rotating the resultant vectors into a common reference frame, the principal pAMS directions show no coring direction dependence.

[10] The pAMS results show a void space susceptibility minimum approximately normal to bedding, with intermediate and maximum susceptibility directions distributed subparallel to this plane. The observed 10–20° angle between the minimum susceptibility and the normal to bedding direction confirms that the pore-fabric geometry is primarily controlled by the macroscopic crossbedding visible in the sandstone.

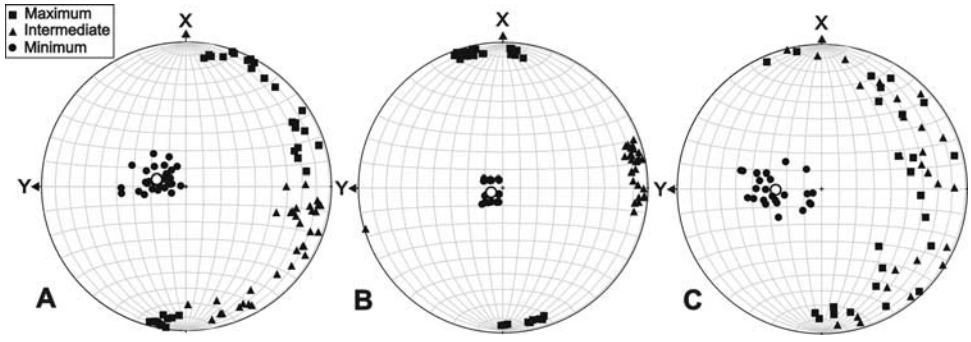

Figure 2. Comparison between principal anisotropy directions as defined by; (A) pAMS, (B) P-wave velocity and (C) S-wave velocity. Open symbols denote average minima (Table 2).

Table 2. mAMS, pAMS, Vp and Vs Anisotropy: Average Directions of Principal Axes[a]

	Magnetic susceptibility (Dry matrix)			Magnetic susceptibility (Ferrofluid saturated)			P-wave velocity (Dry)			S-wave velocity (Dry)		
	Max.	Int.	Min.	Max.	Int.	Min.	Max.	Int.	Min.	Max.	Int.	Min.
Trend	025.9	137.9	301.4	028.8	120.6	281.4	351.4	081.7	248.7	087.4	083.8	269.0
Plunge	14.8	37.4	65.1	04.6	15.7	73.2	01.5	06.5	83.1	30.5	22.4	64.2
Error	16.5	18.9	22.1	10.5	9.1	3.2	1.9	2.7	2.1	-	-	5.3

[a]Error angles were calculated using Fisher (Minima) or Bingham (Intermediate and Maximum) statistics. Minimum directions only are plotted on Figure 2 as open circles. 27 samples used for analysis.

[11] The scatter of the data in Figure 2a, as reflected in the error angles (Table 2), is attributed to the natural variability of the material. Scatter is smallest for the pAMS minimum directions, which are tightly clustered, whilst the intermediate and maximum susceptibility values are distributed along a great circle essentially sub-parallel to the cross-bedding. In detail, however, the two populations of pAMS maximum and intermediate directions are seen to be distinct, with maxima and intermediate sub-parallel to the strike and dip of the cross-bedding, respectively.

[12] P and S-wave velocity data are analysed in a manner similar to the AMS data. In each analysis, 108 velocity measurements (36 from each of three orthogonal cores) are used to determine velocity ellipsoids by applying the general equation for an ellipsoid to the slownesses calculated from the acoustic velocities, using the method of *Louis et al.* [2003]. Each velocity measurement corresponds to a point on the surface of the ellipsoid, given by the orientation of the measurement on the core and the axis of the core. Quality of fit is evaluated by solving the forward problem, yielding a residual error in velocity of $\sim$1.5%, and a concomitant error in principal directions of $\pm 2^\circ$. This velocity model error is approximately equal to the velocity measurement error. Orientations of minimum, intermediate and maximum axes of the resulting velocity ellipsoids have been plotted on stereographic projections in the same way as the pAMS data (Figures 2b and 2c). To allow for statistical analysis, nine cores are used, three in each axis. This gives 27 unique combinations of X, Y, and Z; each of which yields an ellipsoid with three principal directions.

[13] Velocity data produces an average ellipsoid (Table 2) with an alignment similar to the average magnetically derived ellipsoid, with the direction of velocity minimum lying sub-normal to the crossbedding and the maximum and intermediate values distributed in the crossbedding plane. In contrast to the magnetic results, however, the principal P-wave velocity directions are more tightly clustered (Table 2) while the S-wave results are more scattered. This scatter in S-wave data reflects both the difficulty in accurate measurement of S-wave velocities and the complicated interaction between polarized S-waves and an anisotropic pore fabric. As a result, the Bingham statistics are unable to return an error angle for the S-wave maximum and intermediate directions, as these directions display no discernible anisotropy within the bedding plane.

[14] Percent anisotropy ((max-min)/mean x 100) of P and S-waves as calculated from the velocity model can be compared with % anisotropy calculated from pAMS (Table 3). Results yield a ratio of $\sim$5:1 for the relative anisotropy of P-wave and pAMS. Theoretical analyses [*Hudson*, 1975] show that small increases in void space have a disproportionately high effect on elastic wave velocities. Our results are therefore entirely consistent with this.

[15] Finally, permeability data shows the highest values of anisotropy (Table 4), with permeability in the X and Y directions being approximately 240% higher than in the Z direction. Experimental error in permeability is estimated using $\sim$100 sequential permeability measurements to calculate a mean and standard deviation. This method gives an error of between 4 and 9%.

4. Discussion and Conclusions

[16] It is important to note that, although we are comparing pAMS and wave velocity data, these two techniques measure very different petrophysical properties. Void space anisotropy derived from susceptibility can be used as a proxy for global average void space geometry and alignment [*Hrouda et al.*, 2000]. By contrast, velocities are elastic measurements influenced not only by the shape of pores and microcracks, but also their alignment, proportion of cementation and by the crystallographic and geometrical arrangement of minerals in the matrix grains along each wavepath [*Hudson*, 1975; *Berge et al.*, 1992]. In combining velocity measurements along many different wavepaths, an equivalent void space anisotropy ellipsoid can be determined. In analysing the velocity data we have assumed that the spatial variation of the received pulse maps to an ellipsoid. This is only true for a second order symmetric tensor [*Louis et al.*, 2003], whereas elastic anisotropy is strictly only fully described by a fourth rank tensor. However, as previously noted, the error in using the ellipsoidal approximation is less than or equal to the measurement accuracy. Hence, there is essentially no loss of accuracy in our second rank approximation.

[17] A representation of the pore fabric geometry useful for comparing results is the Flinn diagram [*Flinn*, 1962], which plots the length ratio of major to intermediate axes (representing linear fabric contribution) against the length ratio of the intermediate to minor axes (representing planar fabric contribution) of the calculated ellipse (Table 3,

Table 3. pAMS, Vp and Vs Anisotropy[a]

	Linear fabric contribution, %	Planar fabric contribution, %	Overall anisotropy, %
pAMS	1.18 ± 0.25	2.63 ± 0.42	3.75 ± 0.31
Vp	4.89 ± 0.70	15.81 ± 0.76	19.08 ± 0.44
Vs	1.37 ± 0.53	3.54 ± 0.49	4.81 ± 0.61

[a]Average values from 27 ellipsoids.

Table 4. Permeability Anisotropy

Measurement direction	X	Y	Z
Permeability (10^{-18} m^2)	105 ± 6	103 ± 4	43 ± 4

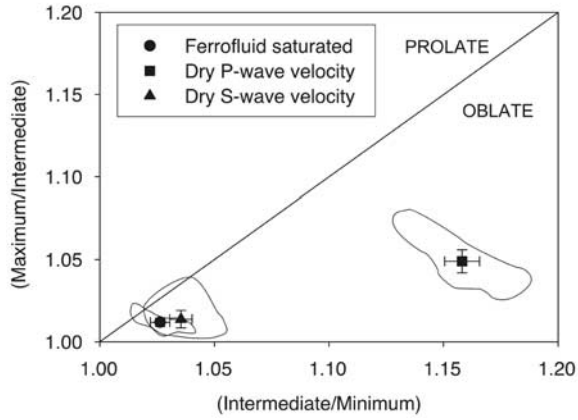

Figure 3. Flinn plot from 27 ferrofluid saturated pAMS ellipsoids, dry V_p and dry V_s ellipsoids. Contours define the bounds of the data, with mean values plotted as solid symbols.

Figure 3). The pAMS, P-wave velocity and S-wave velocity data all indicate that the pore fabric is oblate, as expected for sedimentary rock.

[18] Both pAMS and wave velocity anisotropy techniques are capable of characterizing the pore fabric of rocks in 3-D without prior knowledge of the principal anisotropy directions. However, each method has limitations. The pAMS method measures the bulk susceptibility, which averages pore shape, size and orientation over the sampled volume and would not always be appropriate if the distribution of pore space within the rock was highly heterogeneous. For acoustic anisotropy measurement, the protocol described requires a minimum of three orthogonal cores. There has been some criticism in the past that the use of multiple cores may lead to measurement of heterogeneity rather than the anisotropy [*Rasolofosaon and Zinszner*, 2002]. However, that suggestion needs to take account of the scale of the investigation. We have addressed the problem of heterogeneity by making measurements on multiple cores taken in three orthogonal directions from a single block of sandstone. This allows for comparison of data both between samples cored in the same orientation, and also between measurements made in common directions on cores taken in orthogonal directions. Since we found close agreement between measurements made in the same orientation on different cores, and good clustering of principal anisotropy axes, we conclude that heterogeneity was not a significant problem in this study.

[19] Here, we have studied a rock with a visible sedimentary fabric reflecting the hydrodynamics of the environment in which it was deposited. We have also shown that this visible fabric is present in the internal pore fabric. One strength of the pAMS technique is its ability to quickly detect and identify void space anisotropy in rocks without any obvious fabric, even where the axes of core samples may not lie along principal anisotropy directions. For the sandstone used in this study, we found that the pAMS principal directions were coaxial with the mAMS principal directions within statistical error (Table 2), suggesting that both anisotropies may have been formed by the same sedimentary process.

[20] Fluid permeability exhibited the highest % anisotropy values (Table 4). However, permeability and its anisotropy are highly dependent on effective pressure and the shape of individual voids [*Jones and Meredith*, 1998]. In these experiments, we compare measurements of permeability made at 5 MPa effective pressure with AMS and velocity measurements made at room pressure.

[21] Figure 2 shows that the pAMS and velocity data exhibit similar principal anisotropy directions. This suggests that, for our sample material, the velocity anisotropy was dominated by pore fabric anisotropy. However, there are significant differences (Table 2) in the orientations of principal axes, which reflects the influences of microstructural parameters other than pore fabric, which effects velocity anisotropy but not pAMS. Hence, in general, pAMS is likely to be a better predictor of permeability anisotropy than velocity anisotropy.

[22] **Acknowledgments.** PMB was supported by the UK Natural Environment Research Council (NERC), award NER/S/A/2001/06507. Further support was provided by NERC grant GR9/03963 to PGM and ESP. Crab Orchard sandstone kindly donated by Silvara Stone Co., Crossville, Tennessee. We thank Christian David and an anonymous reviewer whose comments have improved the paper.

References

Ayling, M. R., P. G. Meredith, and S. A. F. Murrell, Microcracking during triaxial deformation of porous rock monitored by changes in rock physical prosperties: I - Elastic wave propagation measurements on dry rocks, *Tectonophysics*, *245*, 205–221, 1995.

Berge, P. A., G. J. Fryer, and R. H. Wilkens, Velocity-Porosity Relationships in the upper Oceanic Crust: Theoretical Considerations, *J. Geophys. Res.*, *97*, 15,239–15,254, 1992.

Birch, F., The velocity of compressional waves in rocks to 10 kilobars, part 1, *J. Geophys. Res.*, *65*, 1083–1102, 1960.

Durrast, H., P. N. J. Rasolofosaon, and S. Seigesmund, P-wave velocity and permeability distribution of sandstones from a fractured tight gas reservoir, *Geophysics*, *67*, 241–253, 2002.

Flinn, D., On folding during 3-D progressive deformation, *Quarterly Journal of the Geological Society of London*, *118*, 385–428, 1962.

Hrouda, F., J. Hanak, and I. Terzijski, The magnetic and pore fabrics of extruded and pressed ceramic models, *Geophys. J. Int.*, *142*, 941–947, 2000.

Hudson, J. A., Overall properties of a cracked solid, *Math. Proc. Camb. Phil. Soc.*, *88*, 371–384, 1975.

Jelinek, V., Statistical processing of anisotropy of magnetic susceptibility measured on groups of specimens, *Studia geoph. geod.*, *22*, 50–62, 1978.

Jones, C., and P. Meredith, An experimental study of elastic wave propagation anisotropy and permeability anisotropy in an illitic shale, Eurock 98, Proc. SPE/ISRM Rock Mechanics in Petroleum Engineering, *1*, 307–314, 1998.

Lo, T.-W., K. B. Coyner, and M. N. Toksoz, Experimental determination of elastic anisotropy of Berea sandstone, Chicopee shale, and Chelmsford granite, *Geophysics*, *51*, 164–171, 1986.

Louis, C. D., C. David, and P. Robion, Comparison of the behaviour of undeformed sandstones in dry and wet conditions, *Tectonophysics*, *370*(1–4), 193–212, 2003.

Pfleiderer, S., and H. C. Halls, Magnetic susceptibility anisotropy of rocks saturated with ferrofluid: a new method to study pore fabric?, *Phys. Earth & Plan. Int.*, *65*, 158–164, 1990.

Pfleiderer, S., and H. C. Halls, Magnetic pore fabric analysis: a rapid method for estimating permeability anisotropy, *Geophys. J. Int.*, *116*, 39–45, 1994.

Rasolofosaon, P. N. J., and B. E. Zinszner, Comparison between permeability anisotropy and elastic anisotropy of reservoir rocks, *Geophysics*, *67*, 230–240, 2002.

Tarling, D. H., and F. Hrouda, The Magnetic Anisotropy of Rocks, Chapman and Hall, London, pp. 217, 1993.

Wyllie, M. R. J., and G. H. F. Gregory, An experimental investigation of factors affecting elastic wave velocities in porous media, *Geophysics*, *23*, 459–493, 1958.

P. M. Benson, P. G. Meredith, and E. S. Platzman, Department of Earth Sciences, University College London, Gower Street, London, WC1E6BT, UK. (p.benson@ucl.ac.uk)